
Article:
Zhu, Z.Q. orcid.org/0000-0001-7175-3307, Pothi, N., Xu, P. et al. (1 more author) (2019) Uncontrolled generator fault protection of novel hybrid-excited doubly salient synchronous machines with field excitation current control. IEEE Transactions on Industry Applications, 55 (4). pp. 3598-3606. ISSN 0093-9994

https://doi.org/10.1109/tia.2019.2909492

Uncontrolled Generator Fault Protection of Novel Hybrid-excited Doubly Salient Synchronous Machines with Field Excitation Current Control

Z. Q. Zhu, N. Pothi, P. L. Xu, and Y. Ren

***Abstract* – In the safe-critical applications such as electric/hybrid electric vehicles, reliability of the machine drive system is vital. Among the various machine fault types, the uncontrolled generator fault (UCGF) at high speed is one of the most serious faults that could damage the machine drive system. In this paper, the fault protection capability of a novel hybrid-excited doubly salient synchronous machine is examined to illustrate its great capability to prevent the dangerous overvoltage issue from the UCGF. PM flux of the novel hybrid-excited doubly salient synchronous machine is inherently short-circuited when the field excitation current is not fed into the excitation windings. Therefore, when the UCGF is detected in the high speed region, the DC-link overvoltage issue can be effectively reduced by forcing the field excitation current to zero. Since only the field excitation current is utilized to protect the machine and power inverter from the UCGF, it is easy to implement and the concept of proposed control strategy can also be applied to other hybrid-excited machines. Finally, the proposed control strategy is verified by both simulation and experimental results on the hybrid-excited doubly salient synchronous machine.**

***Index Terms*-- Fault protection, field excitation current, hybrid excitation, permanent magnet machine, uncontrolled generator fault (UCGF).**

I. INTRODUCTION

ELECTRICAL machines and drives play a vital role in applications of electric, hybrid electric, and fuel cell vehicles. The requirements of an electrical machine for traction applications include: high torque/power density, high torque for starting, low speed and hill climbing, high power for high speed cruising, wide operating speed range, and high efficiency over wide speed and torque ranges, particularly at low torque operation.

Permanent magnet (PM) machines, which exhibit the advantages of high torque/power density, high efficiency, and wide operating speed range [1]-[2], are now widely employed by electric/hybrid electric vehicle (EV/HEV) manufacturers, e.g. Toyota, Nissan, BMW, and even Tesla etc. For PM machines, high speed operation above the base speed is realized by utilizing flux weakening control to suppress the back-EMF produced by PMs.

Since EVs/HEVs are the safe-critical applications, the reliability of the machine drive system has become an increasingly important issue [3]-[5]. Many papers have been presented related to the fault impacts, detections, and fault tolerances for the machines [5]-[11].

Among the various machine fault types, the uncontrolled generator fault (UCGF) at high speed in a PM machine [10]-[15] is one of the most serious faults that could damage the machine and power inverter, which will be particularly discussed in this paper. The UCGF is emerged when the flux-weakening control is unexpectedly disappeared, which usually happens when the switching signals are suddenly removed or the encoder is damaged [10]-[15]. It would be a serious problem if the machine operates at high speed, since the back-EMF in each phase winding, which is usually several times higher than the rated supply voltage, will immediately become a voltage source to deliver the regenerated energy to charge the DC-link capacitor. This higher voltage in the DC-link might explode the capacitor, inverter switches, and even demagnetise the PMs [15], [16]. Although the UCGF has been presented in [10]-[15], these researches focus mostly on the optimization of the machine parameters such as the saliency ratio, PM per-unit flux, and rotor moment of inertia.

On the other hand, the hybrid-excited doubly salient synchronous machine (HEDSSM), which consists of two excitation sources, i.e. permanent magnets (PMs) and DC field windings, Fig. 1 (c), has been introduced in [17]-[28]. Such hybrid-excited machines have the potential to improve the machine flux-enhancing and flux-weakening characteristics, due to their adjustable flux-linkage capability. A high torque at low speed and a wide operating speed range can thus be provided [23]. In addition, due to the fact that all the PMs and windings, i.e. field and armature windings, are located on the stator, it has robust rotor structure and excellent cooling capability. Moreover, HEDSSM can significantly alleviate the issue of overvoltage in the UCGF when an appropriate field excitation current control strategy is utilized. Under the UCGF condition, the flux-linkage and EMF could be reduced when the field excitation current is controlled towards zero or simply remove the field excitation circuit if possible.

In summary, in a conventional wound-field synchronous machine, it is relatively easier to reduce or remove the field excitation in order to avoid high back-emf during high speed faults. In a PM machine, it is usually very challenge to protect the dc link from uncontrolled generator operation due to flux weakening at high speed. Even in hybrid excited machines, it remains a difficult control task if it is not properly considered at the machine design stage, as a result of flux weakening operation at high speed which is often achieved by controlling both

Z. Q. Zhu, Nattapong Pothi, Peilin Xu, and Yuan Ren are with the Department of Electronic and Electrical engineering, The University of Sheffield, UK. (e-mail: z.q.zhu@sheffield.ac.uk, xupeilinnuaa@gmail.com, y.ren@sheffield.ac.uk). Nattapong Pothi is now with School of Engineering, University of Phayao, Phayao, Thailand (e-mail: nattapong.po@up.ac.th).

armature d-axis current and field excitation for high speed operation. In this case, the back-emf during high speed faults could be still too high even if the field excitation is removed. In this paper, it is proposed that together with the novel machine magnetic circuit design, it is possible to simply employ the technique of removing or reducing the field excitation to protect the dc link to avoid high back-emf during high speed faults.

The fault protection capability of the HEDSSM will be examined and its design features will be firstly described in this paper. Removing the field excitation circuit when UCGF happens require additional hardware circuit, and therefore, in this paper, the proper field excitation current control strategy of the hybrid-excited doubly salient synchronous machine is proposed to effectively reduce the dangerous overvoltage from the UCGF. The proposed control strategy is verified by both simulation and experimental results on a prototype hybrid-excited doubly salient synchronous machine.

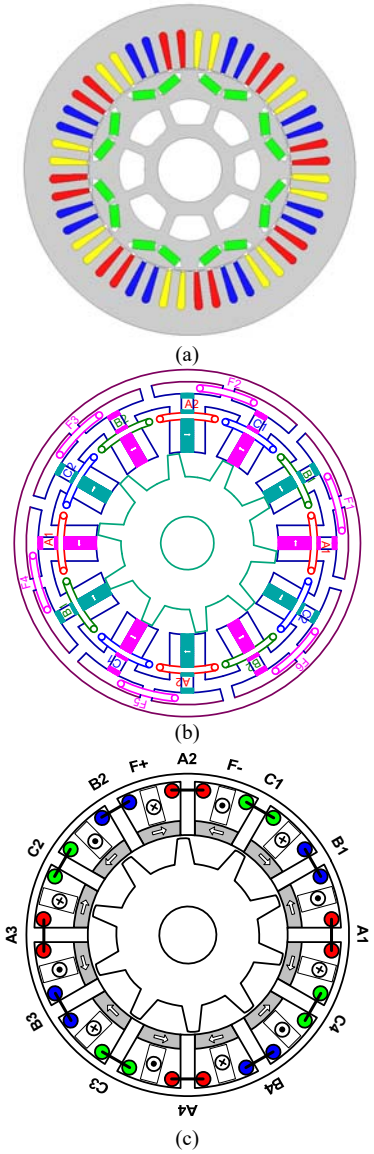

Fig. 1. Cross-section of different PM machine topologies. (a) Conventional IPM machines [30]. (b) Hybrid excited switched flux PM machines [31]. (c) Proposed fault-tolerant HEDSSM [17].

II. Hybrid-Excited Doubly Salient Synchronous Machine

A. Machine Topology and Operating Principle

As mentioned above, permanent magnet (PM) synchronous machines as shown in Fig. 1(a) have been widely used for EV/HEV applications. However, since the magnets are located on the rotor, the PMs may be subjected to high mechanical stress at high speed and may also be difficult to cool. Hence, switched-flux PM machines which have the PMs and the armature windings placed in the stator have been developed [1]. As a result, a robust rotor structure suitable for high speed applications can be obtained, whilst the temperature rise can be more conveniently managed. To further enhance the flux-linkage adjustable capability, the hybrid-excited switched-flux permanent magnet machines, which have two excitation sources, i.e. the PM and the field excitation, are proposed, as shown in Fig. 1(b).

The three-phase 12-stator slot/10-rotor pole HEDSSM is shown in Fig. 1(c) [17], where the PMs are placed between the contiguous slot openings of the stator teeth. Each phase winding consists of four armature coils connected in series. The twelve DC coils are also connected in series to form a single winding. The parameters of the prototype machine are listed in Table I. Since the back-EMF of the prototype machine is nearly zero when the field excitation current is not employed (i_f^*=0), this machine exhibits a fault protection capability based on the control of field excitation current.

The simplified model showing the PM and current flux paths and the flux line distribution of HEDSSM without/with field excitation are shown in Fig. 2. It is clear that without field excitation, PM flux is short-circuited in stator almost without linking with rotor, Fig. 2(a), while with field excitation, more PM flux passes through the rotor, as shown in Fig. 2(b). It should be noted that the hybrid excited switched flux PM machines shown in Fig.1(b) also has similar characteristics. Thus, the techniques to be developed in this paper will be equally applicable to this type of machines, and indeed, the principle developed is applicable to almost any type of hybrid excited PM machines.

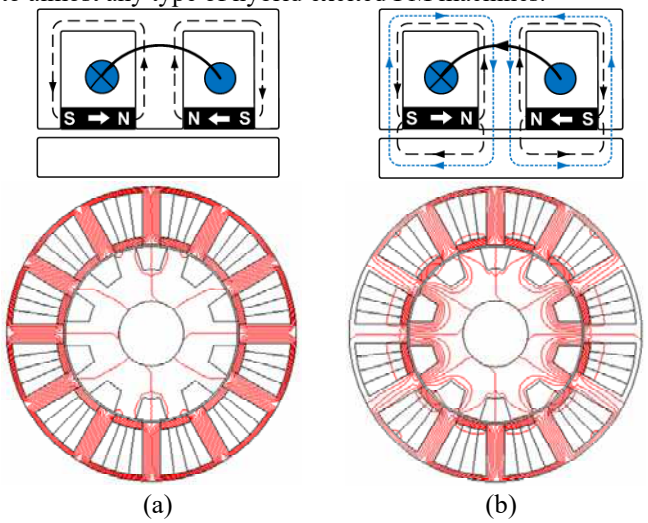

Fig. 2. Simplified model showing the PM and current flux paths and flux line distributions [17], [29]. (a) Without field excitation. (b) With field excitation.

B. *Flux Regulation Capability and Back-EMF*

The phase flux-linkages and back-EMFs against the rotor position of the prototype machine at various specific field excitation currents and at 400 rpm are shown in Fig. 3(a) and (b), respectively. It can be observed that the amplitude of phase flux-linkage can be enhanced with the increase of the field excitation current. It can be seen from Fig. 3 and Fig. 4 that the higher field excitation current, the larger phase flux-linkage and back-EMF can be observed, until the field is over excited, i.e. the flux produced by the field excitation is higher than that of the PM. When the field excitation current is zero (i_f^*= 0), the amplitude of phase flux-linkage is only approximately 0.98 mWb, while the back-EMF is almost zero.

TABLE I
MACHINE PARAMETERS OF PROTOTYPE HEDSSM

Permanent magnet flux	0.98mWb
Number of equivalent pole pairs	10
Packing factor	0.59
Rated DC-link voltage	26 V
Rated torque	0.71 Nm
Rated speed	400 rpm
Peak armature current	7.92 A
Field excitation current	5.6 A
Number of turns per phase of armature winding	184
Number of turns of field winding	552
Armature winding resistance	1 Ω
Field winding resistance	3 Ω
d-axis and *q*-axis inductances	2 mH
Self-inductance of field winding	0.5 mH

It should be noted that when the worse-scenarios arise, such as inverter short-circuit at high speed, the back-EMF of the HEDSSM can be significantly diminished by adopting i_f = 0. Thus, the potential damages of the machine and inverter can be prevented. As a result, the HEDSSMs exhibit significant advantages in terms of fault protection capability compared to the conventional PM machines.

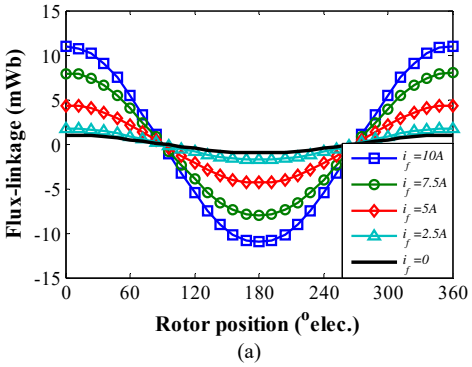

(a)

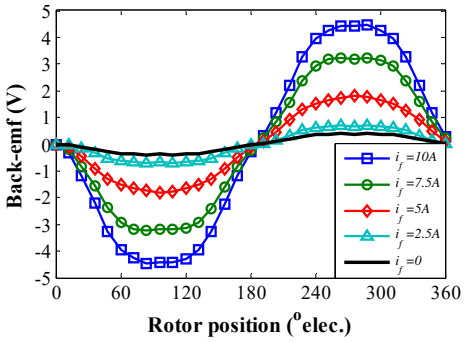

(b)

Fig. 3. Open-circuit characteristic of the prototype machine corresponding to the specific values of field excitation current, in phase A. (a) Flux-linkage (b) Back-EMF.

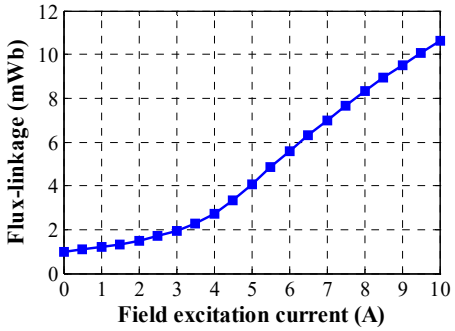

Fig. 4. Flux-linkage amplitude with field excitation current.

C. *Mathematical Model*

The simplified *d*-axis and *q*-axis voltages of the HEDSSM expressed in the synchronous reference frame are given as

$$v_d = R_s i_d + L_d \frac{di_d}{dt} + L_{mf} \frac{di_f}{dt} - \omega L_q i_q \tag{1}$$

$$v_q = R_s i_q + L_q \frac{di_q}{dt} + \omega\left(\psi_{pm} + L_d i_d + L_{mf} i_f\right) \tag{2}$$

Since the flux-linkages are given as $\psi_d = \psi_{pm} + L_d i_d + L_{mf} i_f$ and $\psi_q = L_q i_q$, the torque T_e can be given by (3).

$$T_e = \frac{3}{2} P\left[\left(\psi_{pm} + L_{mf} i_f\right) i_q + \left(L_d - L_q\right) i_d i_q\right]. \tag{3}$$

where i_d, i_q are the *d*-axis and *q*-axis currents, i_f, v_f are the field current and voltage, R_s is the armature resistance, L_{mf}, R_f are the mutual inductance and resistance of field winding, L_d, L_q are the *d*-axis and *q*-axis inductances, ψ_d, ψ_q, ψ_{pm} are the *d*-axis and *q*-axis flux-linkages, and permanent magnet flux-linkage, and ω is the electrical rotor speed.

III. FAULT PROTECTION OPERATION

A. *Uncontrolled Generator Fault*

When the flux-weakening control is unexpectedly disappeared, the EMF in each phase would instantaneously become a large voltage source, which delivers the regenerated current (i_{regen}) back to the DC-link through the

free-wheeling diodes of the inverter switches, as shown in Fig. 5. This fault has been defined as uncontrolled generator fault (UCGF) presented in [10]-[15], which is usually emerged from the removal of switching signals of inverter switches and the damage of the processing unit or position encoder. If the DC-link capacitor cannot absorb the abruptly regenerative energy, the explosion of both capacitor and inverter switches might be unpredictably emerged as caused by the dangerous overvoltage.

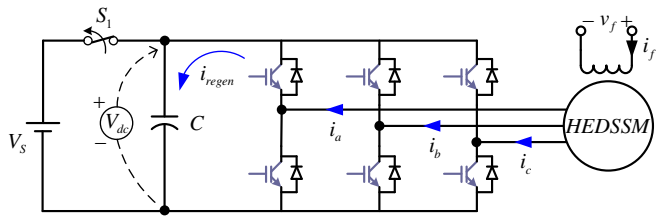

Fig. 5. Uncontrolled generator fault (all gate-signals are removed).

When the UCGF is detected, the EMF in each phase would instantaneously become a large voltage source. Therefore, the switch (S1) is simultaneously controlled to protect the main dc power supply (V_s). The DC-link voltage (V_{dc}) is measured between anode and cathode terminals of the capacitor as shown in Fig. 4. It is noted that since the other overvoltage protections, such as the braking resistance, is not considered in this circuit, the impact of the UCGF can be evaluated considering only the regenerative energy that produced by the machine.

B. *Fault Protection Control Strategy*

As aforementioned above, the HEDSSM has the feature of flux-regulation capability by adjusting the field excitation winding. Therefore, the field winding would be possibly utilized to eliminate the regenerated energy caused by the UCGF, particularly at the high speed flux-weakening operation region.

The fault protection control strategy for the HEDSSM is shown in Fig. 6. In normal operation, as defined in Fig. 6(a), the maximum field excitation current ($i_{f,max}$) is employed in whole operating regions in order to achieve the maximum torque. The *d*-axis current is utilized to weaken the flux-linkage in flux-weakening operation, while the *q*-axis current is determined according to the speed and load-torque as shown in Fig. 6(b). In the UCGF, the DC-link capacitor is rapidly charged by the regenerated current and results in the serious overvoltage. Thus, the DC-link voltage is measured and utilized to activate the fault operation. Practically, when the DC-link voltage is greater or equal to the pre-set maximum DC-link voltage ($V_{dc} \geq V_{dc,max}$), the field excitation current is controlled to zero to protect the drive system (i_f^*= 0). As a result, the overvoltage issued could be solved for the HEDSSM with the proposed control strategy.

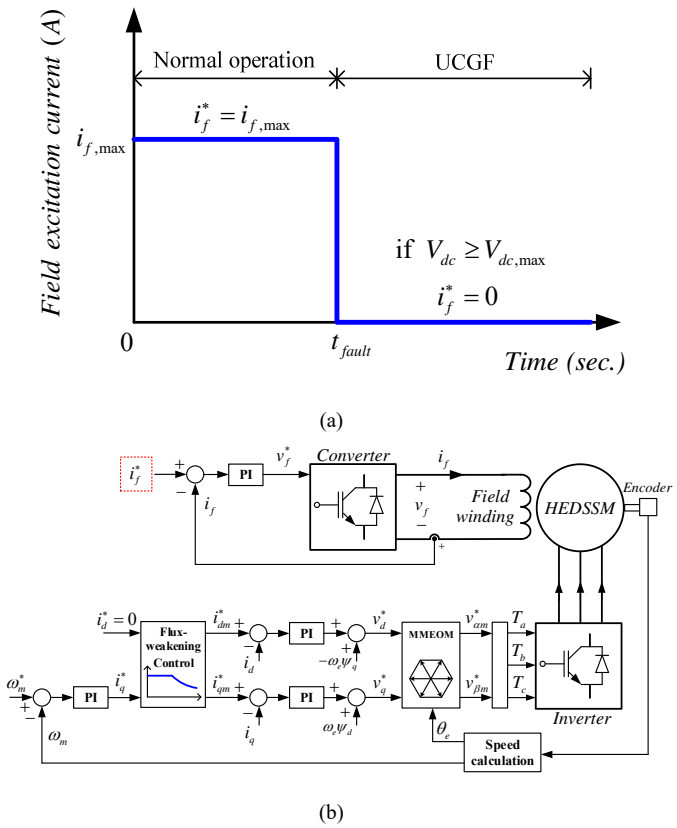

Fig. 6. Fault protection control strategy. (a) Field excitation current control (b) Control block diagram of the HEDSSM.

IV. Verification of Fault Protection Capability

The effectiveness of the fault protection control method is verified by both simulation results and experimental results in this paper on a small prototype HEDSSM.

A. *Simulation Results*

The Simulink@MATLAB is utilized to simulate the UCGF condition and verify the fault protection control. The DC-link voltage is set to 24 V, while the machine reference speed is set to 2,700 rpm, as shown in Table II. The maximum field excitation current is 10 A to enhance the flux-linkage. In order to detect the UCGF, the maximum DC-link voltage ($V_{dc,max}$) is set to 25 V. Other setting parameters are presented in Table II.

TABLE II
Fault Protection Verification Setup

Reference speed	2700 rpm
DC-link voltage (V_{dc})	24 V
Pre-set maximum DC-link voltage ($V_{dc,max}$)	25 V
Maximum armature current	7.92 A
Maximum field excitation current ($i_{f,max}$)	10 A
DC bus capacitance	2,200 μF
Moment of inertia	0.001 kg·m^2

Two field excitation current control strategies of HEDSSM under the UCGF are compared:

(1) Maximum field excitation current in whole regions (i_f^*= 10 A) to simulate the conventional PM machines in which the excitation cannot be changed when UCGF happens.

(2) Maximum field excitation current in normal operation, and zero field excitation current when UCGF detected (i_f^*= 0).

Figs. 7–8 show the simulation results of these two control strategies for HEDSSM.

In normal operation mode, Fig. 7(a), the HEDSSM is operated in the flux-weakening region with the speed at 2,700 rpm. Meanwhile, the maximum field excitation current is used to enhance the torque output, as shown in Fig. 7(b). The amplitudes of line back-EMF of both strategies are at the same level due to the same speed and flux-linkage, as shown in Fig. 7(c) and (d) before the UCGF.

The UCGF is set to emerge at 2.0 s. In the UCGF mode, the machine speeds for both strategies are significantly decreased, Fig. 7(a). It should be noted that the prototype machine can coast down quickly due to its small moment of inertia, as shown in Fig. 7(a). The load torque is set as a constant value in the simulation system. Hence, the speed responses show in a linear drop way, Fig. 7(a). It should be emphasized that the proposed UCGF protection method for the developed HEDSSM still works even if the speed is not reduced since without field excitation, the magnetic circuit is short-circuited and consequently the back-emf is almost zero at any speed. For the control strategy utilizing the maximum field excitation current in the whole region (i_f^*= 10 A), the DC-link voltage is rapidly increased by around 22 V (~88.0%), as shown in Fig. 8(c). Under this condition, the DC-link capacitor is quickly charged by the regenerated current from the machine, which corresponds to the *d*- and *q*-axis current variations as shown in Fig. 8(a).

When the DC-link voltage is greater than or equal to 25 V, as defined in Table II, the UCGF is detected. The field excitation current is then controlled to zero (i_f^*= 0), as shown in Fig. 7(b). The line back-EMF can be visibly decreased, as shown in Fig. 7(d), compared to the results of the strategy that utilizes the maximum field excitation current in whole regions in Fig. 7(c). Therefore, the regenerated current of the HEDSSM can be significantly reduced corresponding to the *d*-axis and *q*-axis currents as shown in Fig. 8(b) and (c), respectively. In addition, the effectiveness of the proposed fault protection control method can be clearly proved by the power storage of the capacitor, as shown in Fig. 8(d). Since the power storage in capacitor is proportional to the square of DC-link voltage, therefore, the trend of this power storage in capacitor is similar to that of DC-link voltage, as shown in Fig. 8, i.e. a peak of the regeneration power is also observed once the UCGF occurs, but it can be quickly reduced with zero field excitation current (i_f^*= 0).

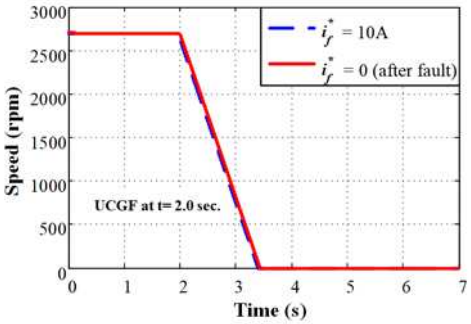

(a)

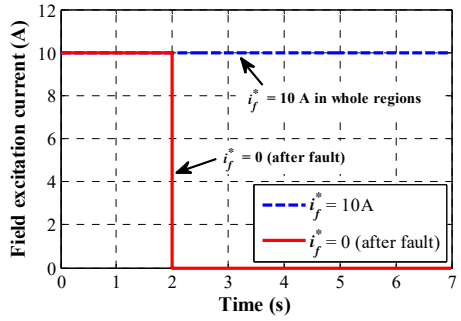

(b)

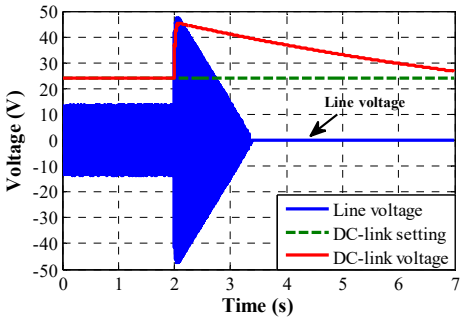

(c)

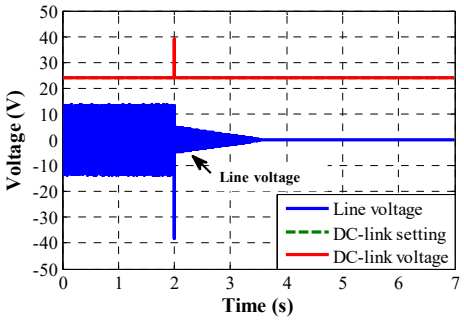

(d)

Fig. 7. Simulation results of the proposed fault protection method (i_f^*= 0) compared to the method utilizing the maximum field excitation current for all regions (i_f^*= 10 A). (a) Speed, (b) Field excitation current control, (c) Line voltage (i_f^*= 10 A), (d) Line voltage (i_f^*= 0 after UCGF).

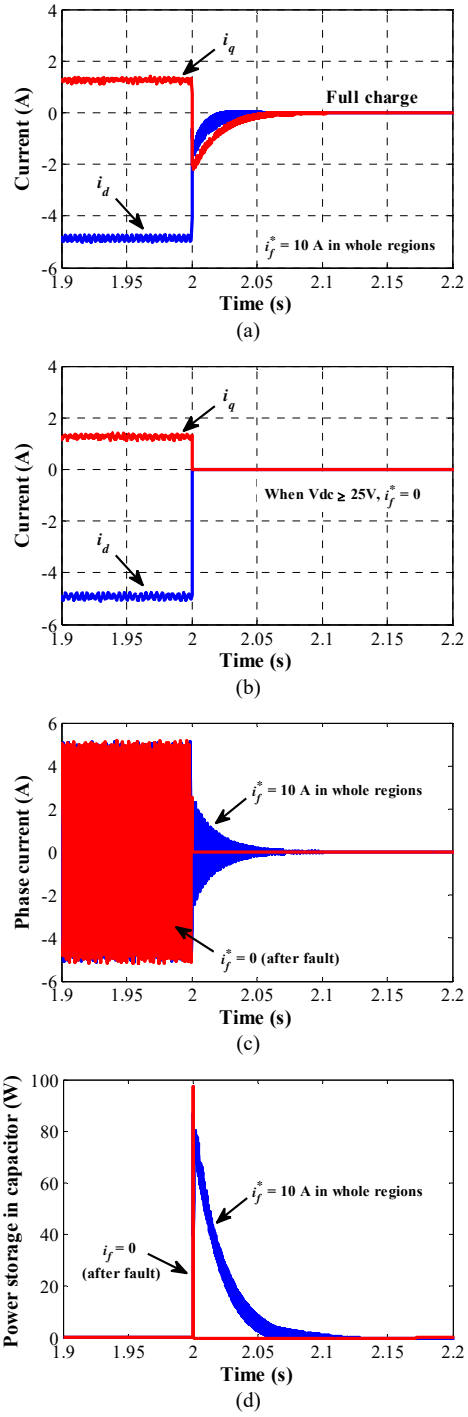

Fig. 8. Simulation results, currents and power storage in capacitor, of the proposed fault protection method (i_f^*= 0) compared to the method that utilising the maximum field excitation current in whole regions (i_f^*= 10 A). (a) *d*- and *q*-axis currents (i_f = 10 A), (b) *d*- and *q*-axis currents (i_f = 0 after UCGF), (c) Armature current, (d) Power storage in capacitor.

B. *Experimental Results*

The prototype HEDSSM, as shown in Fig. 9(a), is controlled by the vector control which is implemented on a dSPACE platform. The prototype machine is connected to a 1.5 kW wound field type DC machine, which is utilized to regulate the load-torque through an external resistance to dissipate the generated power. The three-phase voltage source inverter (VSI) is utilized with the SVPWM technique, while the field excitation current is regulated by the step-down DC-DC converter, as illustrated in Fig. 9(b). To improve the tracking accuracy of the field excitation current, the feed-back current control with the proportional and integral (PI) regulators is considered. The experimental platform is shown in Fig. 9(c). The experimental setup parameters are defined in Table II. To generate the UCGF in the experiment, all switching gate-signals are suddenly removed at the speed of 2700rpm.

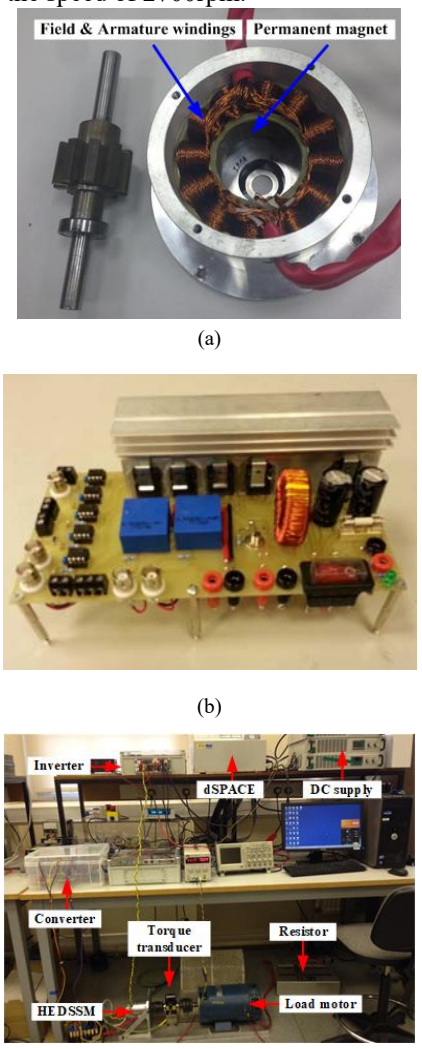

Fig. 9. Experiment platform. (a) Prototype HEDSSM, (b) DC-DC (step-down) converter, (c) Test-rig.

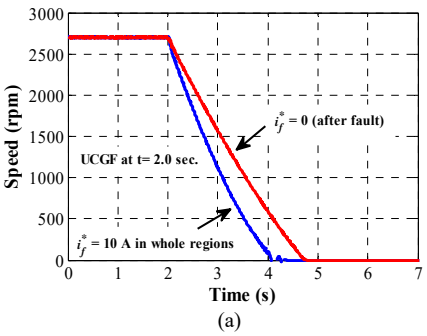

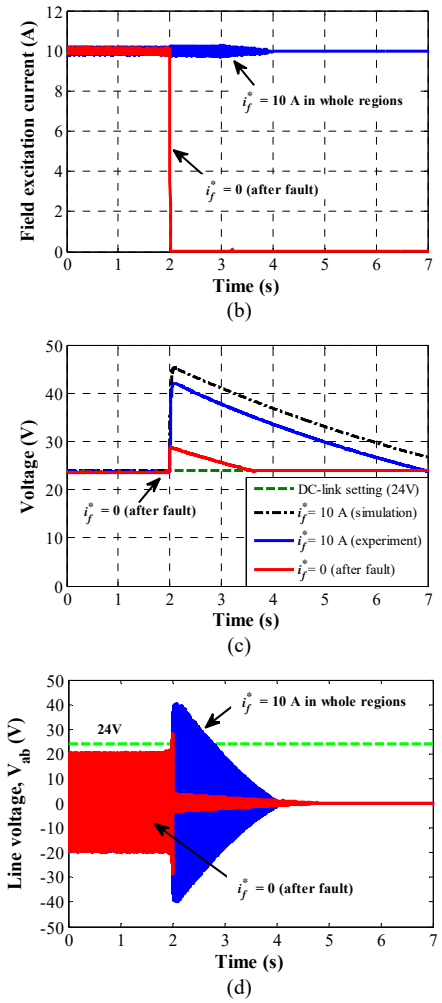

Fig. 10. Experimental results of the proposed fault protection method (i_f^*= 0) compared to the method utilizing the maximum field excitation current in whole regions (i_f^*= 10 A) (a) Speed, (b) Field excitation current control, (c) DC-link voltage, (d) Line voltage.

Figs. 10-11 show the experimental results of the proposed fault protection method (i_f^*= 0) compared to the method utilizing the maximum field excitation current in whole regions (i_f^*= 10 A). The measured speed and field excitation current are shown in Fig. 10(a)-(b), respectively. It is obvious that these results exhibit similar trends as the simulation results. On the other hand, the field excitation current i_f^*=10A is used in the conventional method, which results in higher copper loss and core loss. Therefore, the speed drops quickly than the method that utilizing i_f^*=0, as illustrated in Fig. 10(a). Moreover, since a permanent magnet DC motor is mechanically coupled to the prototype machine, and is connected with an adjustable power resistor to provide the load, as shown in Fig. 9(c), the load torque is proportional to the machine speed. At the same time, the core loss in high speed is higher than that in low speed. These two reasons makes the speed of both methods drop much quickly in high speed, as shown in Fig. 10(a).

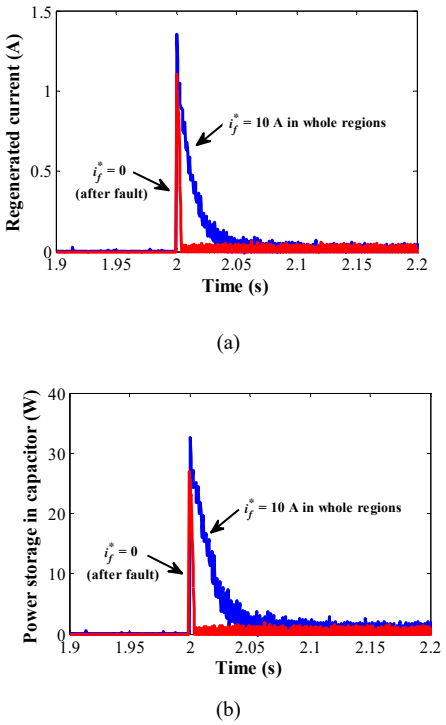

Fig. 11. Measured regenerated current and power storage in capacitor of the proposed fault protection method (i_f^*= 0) compared to the method that utilising the maximum field excitation current in whole regions (i_f^*= 10 A). (a) Regenerated current, (b) Measured power storage in capacitor.

The UCGF happens at the instant of 2.0 s. Under the UCGF condition, since the flux-density of the method that utilizing i_f^*= 10 A is higher than the method that utilizing i_f^*= 0 due to the field excitation flux resulting in the higher core loss [27], the speed of the method that utilizing i_f^*= 10 A is falling quickly than the method that utilizing i_f^*= 0, as illustrated in Fig. 10(a).

It is obvious that for the control strategy utilizing the maximum field excitation current in the whole region (i_f^*= 10 A), the measured DC-link voltage is speedily increased by around 19 V (~79.16%), as shown in Fig. 10(c). Meanwhile, the overvoltage in the DC-link capacitor can be eliminated based on the proposed method (i_f^*= 0). Likewise, the effectiveness of the fault protection capability of the HEDSSM can be clearly proved by the comparison of measured line voltage (V_{ab}), as shown in Fig. 10(d). The regenerated current and power storage in the capacitor are shown in Fig. 11(a)-(b), respectively.

It should be noted that, in the proposed method, it takes a short time for the DC-link voltage to drop back to normal levels after the fault, Fig. 10(c). This is because of the existence of the system delay in the field current control loop, which makes the simulation results and experimental results slightly different. Nevertheless, if the field excitation circuit can be removed instantaneously (with the employment of additional hardware circuit) once UCGF happens, a good match could be expected between the simulation and experimental results.

V. Conclusion

This paper has described the novel features of a hybrid-excited doubly salient synchronous machine (HEDSSM) and examined its fault protection capability based on the field excitation current control strategy under the UCGF conditions. These results have shown that the developed fault-tolerant HEDSSM can considerably alleviate the issue of overvoltage by utilizing zero field excitation current control (or simply removing field excitation circuit if possible) when the UCGF is detected. The proposed fault protection control strategy for the HEDSSM is simple to implement as only the field excitation current control is utilized, and can be also applied to other hybrid-excited machines. It has clearly demonstrated that it is very important to consider both the machine magnetic circuit design and the fault control in order to mitigate the issues with UCGF.

It should be pointing out that due to the existence of the field winding, additional copper loss is introduced into the machine, and consequently, the total loss is increased compared to the conventional machine which has only armature windings. Since there are two types of currents, i.e. field current and armature current, which can be used to weaken the flux-linkage, in the high speed region, the optimal values of field current and armature current could be employed to minimize the total copper loss in the machine and then improve the machine efficiency.

VI. References

[1] M. Cheng, W. Hua, J. Zhang, and W. Zhao, "Overview of stator permanent magnet brushless machines," *IEEE Trans. Ind. Electron*., vol. 58, no. 11, pp. 5087-5101. Nov. 2011.

[2] Z. Q. Zhu and D. Howe, "Electrical machines and drives for electric, hybrid, and fuel cell vehicles," *Proc. IEEE*, vol. 95, no. 4, pp. 746–765, Apr. 2007.

[3] Z. Q. Zhu, K. Utaikaifa, K. Hoang, Y. Liu, and D. Howe, "Direct torque control of three-phase PM brushless AC motor with one phase open circuit fault," in *Proc. IEEE Int. Conf. Elect. Mach. Drives*, May 3-6, 2009, pp. 1408–1415.

[4] J. O. Estima and A. J. M. Cardoso, "Performance analysis of permanent magnet synchronous motor drives under inverter fault conditions", in *Proc. 18th Int. Conf. Elect. Machines (ICEM)*, Sep. 2008, pp. 1-6.

[5] Y.S. Chen, Z. Q. Zhu, and D. Howe, Fault analysis of pm of brushless ac under field-weakening operation, *Proc. 32th University Power Engineering Conference (UPEC)*, UMIST, pp.41-44, 1997.

[6] A. M. El-Refaie, "Fault-tolerant permanent magnet machines: a review," *IET Elect. Power Appl*., vol. 5, no. 1, pp. 59–74, Jan. 2011.

[7] M. T. Abolhassani and H. A. Toliyat, "Fault tolerant permanent magnet motor drives for electric vehicles," in *Proc. IEEE Int. Electric Machines & Drives Conf. (IEMDC)*, 2009, pp. 1146–1152.

[8] R. R. Errabelli and P. Mutschler, "Fault-tolerant voltage source inverter for permanent magnet drives," *IEEE Trans. Power Electron*., vol. 27, no. 2, pp. 500–508, Feb. 2012.

[9] C. Liu, K. T. Chau, and W. Li, "Comparison of fault-tolerant operations for permanent-magnet hybrid brushless motor drive," *IEEE Trans. Magn*., vol. 46, no. 6, pp. 1378–1381, Jun. 2010.

[10] S. H. Han, T. M. Jahns, M. Aydin, M. K. Guven, and W. L. Soong, "Impact of maximum back-emf limits on the performance characteristics of interior permanent magnet synchronous machines," in *Rec. of 2006 IEEE Industry Applications Society Annual Meeting*, Vol. 4, Oct. 2006, pp. 1962 – 1969.

[11] B. A. Welchko, T. A. Lipo, T. M. Jahn, and S. E. Schulz, "Fault tolerant three-phase AC motor drive topologies: A comparison of features, cost, and limitations," *IEEE Trans. Power Electron*., vol. 19 no. 4, pp. 1108-1116, Jul. 2004.

[12] T. M. Jahns and V. Caliskan, "Uncontrolled generator operation of interior PM synchronous machines following high speed inverter shutdown," *IEEE Trans. Ind. Appl*., vol. 35, no. 6, pp. 1347–1357, Nov./Dec. 1999.

[13] G. Pellegrino, A. Vagati, and P. Guglielmi, "Design tradeoffs between constant power speed range, uncontrolled generator operation, and rated current of IPM motor drives," *IEEE Trans. Ind. Appl*., vol. 47, no. 5, pp. 1995–2003, Sep./Oct. 2011.

[14] C. Z. Liaw, W. L. Soong, B. A. Welchko, and N. Ertugrul, "Uncontrolled generation in interior permanent-magnet machines," *IEEE Trans. Ind. Appl*., vol. 41, no. 4, pp. 945–954, Jul./Aug. 2005.

[15] G. Choi, T. M. Jahns, "Interior permanent magnet synchronous machine rotor demagnetization characteristics under fault conditions", *Energy Conversion Congress and Exposition (ECCE)*, *2013 IEEE*, pp. 2500-2507, Sept. 2013.

[16] T. Sun, S. H. Lee, and J. P. Hong, "Faults analysis and simulation for interior permanent magnet synchronous motor using Simulink@MATLAB", in *Proc. Int. Conf. on Elect. Mach. & Syst. (ICEMS)*, Oct. 8-11, 2007, pp. 900-905

[17] I. A. A. Afinowi, Z. Q. Zhu, Y. Guan, J. C. Mipo, and P. Farah, "Hybrid-excited doubly salient synchronous machine with permanent magnets between adjacent salient stator poles," *IEEE Trans. Magn*., vol. 51, no. 10, pp.1-9, Oct. 2015.

[18] Y. Amara, L. Vido, M. Gabsi, E. Hoang, A. H. B. Ahmed, and M. Lecrivain, "Hybrid excitation synchronous machines: energy-efficient solution for vehicles propulsion," *IEEE Trans. Veh. Technol., vol. 58, no. 5*, pp. 2137-2149, Jun. 2009.

[19] R. L. Owen, Z. Q. Zhu, and G. W. Jewell, "Hybrid-excited flux-switching permanent-magnet machines with iron flux bridges," *IEEE Trans. Magn*., vol. 46, no. 6, pp. 1726-1729, Jun. 2010.

[20] J. T. Chen, Z. Q. Zhu, S. Iwasaki, and R. Deodhar, "A novel hybrid-excited switched-flux brushless AC machine for EV/HEV applications," *IEEE Trans. Veh. Technol*., vol. 60, no. 4, pp. 1365-1373, May. 2011.

[21] K. Yamazaki, K. Ando, K. Nishika, K. Shima, T. Fukami, and K. Shirai, "Assist effects of additional permanent magnets in salient-pole synchronous generators", in *XIX International Conference on Electrical Machines* (*ICEM*), Rome, pp. 1-6, 2010.

[22] L. R. Huang, Z. Q. Zhu, and W. Q. Chu, "Optimization of electrically excited machine for electrical vehicle applications considering load condition," *The 8th International Conference on Power Electronics, Machines and Drives (PEMD 2016),* 19-21 April 2016, Glasgow, UK.

[23] N. Pothi, Z. Q. Zhu, I. A. A. Afinowi, B. Lee, and Y. Ren, "Control strategy for hybrid-excited switched-flux permanent magnet machines," *IET Electr. Appl*., vol. 9, no. 9, pp. 612–619, 2015.

[24] Y. Liu, Z. Zhang, and X. Zhang, "Design and optimization of hybrid excitation synchronous machines with magnetic shunting rotor for electric vehicle traction applications," *IEEE Trans. Ind. Appl.*, vol. 53, no. 6, pp. 5252-5261, Nov./Dec. 2017.

[25] Q. Wang, S. Niu, and X. Luo, "A novel hybrid dual-PM machine excited by AC with DC bias for electric vehicle propulsion," *IEEE Trans. Ind. Electron.*, vol. 64, no. 9, pp. 6908-6919, Sept. 2017.

[26] Z. Q. Zhu, I. A. A. Afinowi, Y. Guan, J. C. Mipo, and P. Farah, "Hybrid-excited stator slot permanent magnet machines-influence of stator and rotor pole combinations," *IEEE Trans. Magn.*, vol. 52, no. 2, pp. 1-10, Feb. 2016.

[27] J.-P. Lee, S.-C. Han, Y.-H. Han, and T.-H. Sung, "Loss characteristics of SFES with amorphous core for PMSM," *IEEE Trans. Appl. Supercond*., vol. 21, no. 3, pt. 2, pp. 1489–1492, 2011.

[28] Z. Q. Zhu, N. Pothi, P. L. Xu, and Y. Ren , "Uncontrolled generator fault protection of novel hybrid-excited permanent magnet machines utilizing field excitation current control," Int. Conf. on Electrical Machines *(ICEM 2018), Alexandroupoli, Greece,* 3-6 Sept. 2018.

[29] I. A. A. Afinowi, Z. Q. Zhu, Y. Guan, J. Mipo, and P. Farah, "A novel brushless ac doubly salient stator slot permanent magnet machine," *IEEE Trans. Energy Convers*., vol. 31, no. 1, pp. 283-292, Mar. 2016.

[30] E. Hoang, M. Lecrivain, and M. Gabsi, "A new structure of a switching flux synchronous polyphased machine with hybrid excitation," *European Conference on Power Electronics and Applications (EPE 2007), Aalborg, Denmark* pp. 1-8, 3-6 Sept. 2007.

[31] T.A Burress, S.L Campbell, C.L Coomer, C.W. Ayers, A. A. Wereszczak, J.P. Cunningham, L.D. Marlino, L.E. Seiber and H.T. Lin, "Evaluation of the 2010 Toyota Prius hybrid synergy drive system," *Oak Ridge National Laboratory report*, March 2011.

Z.Q. Zhu (F'09) received the B.Eng. and M.Sc. degrees in electrical engineering from Zhejiang University, Hangzhou, China, in 1982 and 1984, respectively, and the Ph.D. degree in electrical engineering from the University of Sheffield, Sheffield, U.K., in 1991. Since 1988, he has been with the University of Sheffield, where he is currently the Royal Academy of Engineering/Siemens Research Chair and is the Head of the Electrical Machines and Drives Research Group, the Academic Director of Sheffield Siemens Wind Power Research Centre, the Director of Midea Electrical Machines and Controls Research Centre, and the Director of the CRRC Electric Drives Technology Research Centre. His current major research interests include the design and control of permanent-magnet brushless machines and drives for applications ranging from automotive to renewable energy.

Nattapong Pothi received the B.Eng. and M.Eng. degrees in electrical engineering from Chiang Mai University, Chiang Mai, Thailand, in 2002 and 2006, respectively, and the PhD degree in 2016 from the University of Sheffield, Sheffield, U.K. He is currently lecturing at School of Engineering, University of Phayao, Phayao, Thailand. His research interests are in the areas of electric drives, energy conversion systems, and power electronic applications.

P. L. Xu (S'15) received the B.Eng. and M.Sc. degrees in electrical and electronic engineering from Nanjing University of Aeronautics and Astronautics, Nanjing, China, in 2010 and 2013, and the Ph.D. degree from the Department of Electronic and Electrical Engineering, University of Sheffield, Sheffield, U.K., in 2017, respectively. He is currently working at Midea Shanghai Electrical Machines and Controls Centre, Shanghai, China. His research interests are the electromagnetic analyses and designs of PM machines and sensorless control techniques.

Yuan Ren (M'17) received the B.Eng. and M.Sc. degrees in electrical and electronic engineering from Zhejiang University, Hangzhou, China, in 2009 and 2012, respectively, and the Ph.D. degree in electrical engineering from the University of Sheffield, Sheffield, U.K., in 2016. Since 2016, he has been a KTP Associate between Dynex Semiconductor, Ltd., Lincoln, U.K., and the University of Sheffield. His research interests include power devices, electrical machines, and control strategies for electric vehicles.